

Slum Terrain Mapping Using Low-Cost 2D Laser Scanners

Syed Riaz un Nabi Jafri*, Tariq Rehman, Asif Ahmed, Muhammad Shahzad Siddiqi, Asad Hayat, Tehniyat Saeed

Department of Electronic Engineering, NED University of Engineering and Technology, University Road, Karachi, Pakistan

*riazun1036@neduet.edu.pk, tariqrehman@neduet.edu.pk, asifmemon@iiee.edu.pk, shahzadsiddiqi@gmail.com, asad.hayat71@gmail.com, engrtehniyat@gmail.com

Abstract—This paper presents a motorbike-based custom made scanning and mapping system for surveying slums and highly populated urban regions. These vicinities are difficult to reach through standard vehicular scanning systems and require a compact solution as presented in this paper. The system consists of two small range 2D Hokuyo laser scanners mounted in right angle orientations to capture the environment. In addition, the global positioning system, the wheel encoder, the inertial measurement unit, and cameras have been integrated with the system to estimate the pose and visual information. Sensorial information has been used to localise the system using Kalman Filtering. Later, by applying the standard transformations, the 3D point cloud map of the surveyed vicinity has been developed. The scanning system has been tested at various locations including densely populated and slum regions. Precise and detailed 3D mapping results have been obtained, which are further extensively analysed to understand the built structure and the road furniture. The working of the system is found to be quite economical and faster than that of local urban surveying systems.

Index Terms—Simultaneous localisation and mapping; IMU; 3D point cloud; 2D laser scanner; GPS.

I. INTRODUCTION

The global population trend shows a significant increase in concentration in urban areas, particularly in the South Asian region. The location of this population is closely related to the existence of socio-economic opportunities [1]. However, as urbanisation progresses, it can put a burden on the resources of these metropolitan areas, resulting in a disparity between population distribution and the availability of fundamental services and infrastructure. To address this challenge, proper planning and administration, based on the most recent information on urban infrastructure and development, are required. In developed nations, regular inspections are performed using cutting-edge equipment such as laser scanners and vision sensors mounted on stationary or wheeled platforms [2]. The data collected from these inspections are used to create 3D maps depicting roadways, bridge structures, building shapes, and slum geometry. These maps are then compared with the

original plans to guide proper planning and improvements in overcrowded areas. On the other hand, underdeveloped countries are still using traditional survey methods that are slow and often produce limited results.

Laser scanning and mapping systems have a long history, originally limited to defence, space, and government applications [3]. In the late 1980s, it was first commercially used for cultural heritage purposes and later developed by companies such as Cyrax and Riegl for stationary scanning and surveying systems [4]. With the advent of new advances in sensors and computer technology, long distance survey methods have been invented using mobile mapping systems that can be mounted on cars, drones, backpacks, and robots [5]. In the current era, the top manufacturers of commercially available mobile laser scanning systems are Riegl, Optech, Trimble, Topcon, and Leica, all of whom offer surveying solutions for various kind of environments [6].

However, these systems are larger in size and require significant space to mount on moving vehicles at a greater cost. Therefore, this research work introduces a custom made slim mobile scanning and mapping system designed to generate 3D digital maps of the surveyed area using a motorbike, as depicted in Fig. 1. The digital information collected through this kind of system is highly valuable in categorising roadways, vegetation, building geometry, and other related features. It is also useful for inspecting built structures, surveying historical sites, evaluating industrial safety, and conducting risk analysis for pre-existing structures [7]. The most suitable laser scanners for compact size of surveying systems are 3D Velodyne, 2D SICK, and Hokuyo scanners.

3D Velodyne scanners offer medium range sensing with a rugged design suitable for various applications [8]. Due to their high cost and heavy computational requirements, they are rarely in use for low-budget mobile and aerial mapping applications. SICK scanners are favoured for mapping and range because of their durable housing and variety of features for indoor or outdoor surveying tasks at moderate prices [9]. On the other hand, Hokuyo scanners exhibit a compact and cost-effective sensing mechanism that makes them suitable for economical scanning systems [10]. Researchers have used the Simultaneous Localisation and

Manuscript received 13 January, 2023; accepted 4 April, 2023.

This research is supported by the Higher Education Commission (HEC), Pakistan under Grant No. TDF-02-057.

Mapping (SLAM) technique to perform mapping projects using a low price 2D Hokuyo scanner [11]. A group of researchers have evaluated indoor mapping outcomes using the trolley-based platform equipped with onboard sensors and computing capabilities [12]. Besides the trolley-based systems, to perform scanning tasks on uneven surfaces such as floor stairs or rough outdoor terrain, many research works have combined several Hokuyo 2D laser scanners with additional dead reckoning sensors on backpack systems to create 2D/3D models of the environment [13]. Similar scanning techniques have been adopted on car-based mobile mapping systems for outdoor forestry surveys by integrating the Hokuyo scanner with Real Time Kinematic Global Navigation Satellite System (RTK-GNSS) module [14]. Google cartographer mapping has been applied by researchers on an autonomous surface vehicle equipped with Hokuyo and Inertial Measurement Unit (IMU) for coastal surveying applications [15].



Fig. 1. (a) Custom made motorbike scanning system and (b) its utilisation.

In contrast to referred research works, the surveying and mapping applications for smaller autobikes have been under investigation all around the globe. In [16], a research group presented a sensor fusion-based localisation and mapping solution for quad bike vehicle. Some researchers [17] performed experiments on multiple SLAM algorithms to investigate bike performance on various outdoor tracks to testify the real time smart bike application. In the same domain, in [18], the authors presented the development of scanner-based system for safe transportation of the electric bicycle and to generate runtime alerts for riders in case of a pothole detected on road surface. In [19], a team of researchers presented the development of a 3D point cloud map and the tracking of the pose of the two-wheeled vehicle using Extended Kalman Filter (EKF). The filter predicted the system state through IMU data and updated the state periodically through multi-layer laser scanner data. In [20], another research group developed the compact scanning and mapping system using a SICK scanner mounted on the two-wheeled platform. Successful feature mapping has been demonstrated using FastSLAM approach within the campus.

In continuation of the fascinating research works presented, this study introduces a unique prototype model of a mobile mapping system mounted on a motorbike. The developed compact prototype has been installed on the back

stand of the bike, allowing the surveyor to effortlessly ride the vehicle while performing scanning tasks, particularly on rough and narrow terrains. The prototype features efficient 2D Hokuyo 30LX scanners, which were selected for their compact design, lightweight, and affordable cost.

This article is organised into several sections. Section II outlines the mechanical design and the instrumentation scheme. Section III provides information on the localisation algorithm and the generation of point cloud maps. Section IV presents the real test results, and finally, the conclusions and the acknowledgement are presented.

II. DESIGN OF THE MOTORBIKE SCANNING SYSTEM

Designing of a motorbike scanning system involves selection of a suitable laser scanner, appropriate placement of multiple scanners at its core, along with the development of mechanical and instrumentation hardware as discussed in the following sections.

A. Mechanical Model

To manufacture the motorbike-based scanning hardware for outdoor mapping, at the first stage, a mechanical model of the system has been designed in AutoCAD software, as shown in Fig. 2(a). The scanning system has been mainly composed of a metal box and its supporting metal base plate. The metal box has been designed to interface all the sensors with it. The supporting plate has been used to rigidly mount the box on some platform and to provide a covering to the installed sensors. After the simulated design has been finished, the actual fabrication of the system has begun. The sensor box has been manufactured using the stainless-steel sheet of thickness 0.1 cm and necessary mechanical operations have been performed on it to install the required sensors. The supporting plate has been manufactured with the same stainless steel sheet and necessary drilling has been carried out for making mounting holes. The fabricated system is shown in Fig. 2(b).

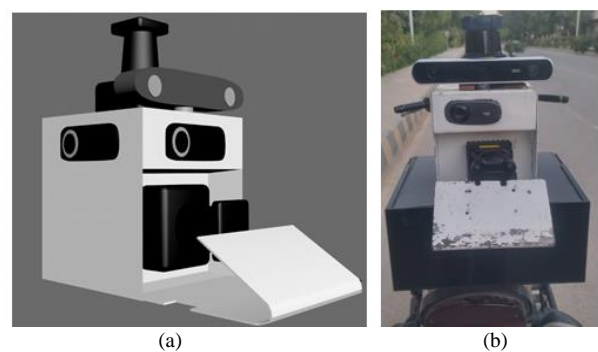


Fig. 2. Design and development of a motorbike scanning system: (a) Mechanical model of the system; (b) Fabricated system.

The sensor box, along with the supportive plate, has been integrated in an acrylic rectangular box. The acrylic box has been manufactured to serve as a housing for batteries, electronic circuitry, and a small embedded board for interfacing scanners and other sensors. It has been integrated with the back stand of the motorbike through removable joints. Finally, both 2D Hokuyo 30LX scanners have been integrated with the sensor box in horizontal and vertical directions. The XSENSE inertial IMU has been

installed inside the box at the middle location. The same sensor has an embedded Global Positioning System (GPS) receiver. Three HD cameras have been installed to capture the visual information about the surrounding. An additional stereo camera has been installed on top surface of the box to sense the motion of the scanning system through its images. The overall design of the scanning system has kept it simple, low-cost, and easy to install. The provision to integrate additional sensors is possible if needed on free surfaces of the sensor box.

B. Instrumentation System Design

Electronic instrumentation circuitry consists mainly of two batteries and three power converter modules to provide the required energy to the scanners and sensors. Both laser scanners have been interfaced to network port of the laptop while the IMU and all cameras have been interfaced through USB ports of the laptop. The Robot Operating System (ROS) packages have been utilised to connect all scanners and sensors to the laptop. The complete block diagram of the system is shown in Fig. 3. The horizontal laser scanner has been used to scan the XY plane of the vicinity and its live data have been utilised to run the open source SLAM ROS package to produce 2D pose and the map. All online data streams of all scanners have been saved along with 2D pose and map information using the ROS bag package during the surveying operation of the respective vicinity. In the instrumentation scheme, the IMU has been connected through the respective ROS package for data logging. All three HD cameras have also been interfaced to ROS and live images have been viewed online in RVIZ package and in parallel stored in respective bag file. Finally, the stereo camera has been connected to ROS and with the relevant package, its computational data along with images have been stored in the bag file.

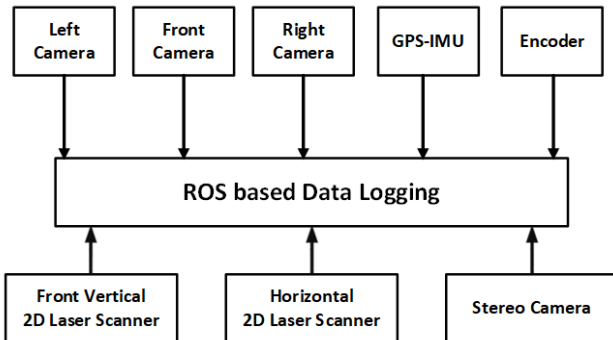


Fig. 3. Instrumentation system design.

The instrumentation strategy follows the unique placement of all sensors as per the assigned reference, as shown in Fig. 4. The cyan reference axis indicates the world reference for any surveying task. The red reference $X_V Y_V$ axis shows the vehicle (motorbike) local axis, which will change its pose w.r.t. the world reference during the vehicle motion. The yellow $X_I Y_I$ axis indicates the IMU-GPS local reference frame. While the blue $X_L Y_L$ axis shows the horizontal laser scanner and stereo camera local frames.

After finishing the surveying and scanning task, all the stored ROS bag data file has been processed in offline mode

using MATLAB scripting, as shown in Fig. 5.

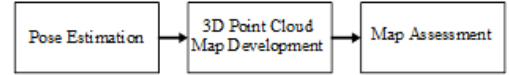


Fig. 5. Offline processing steps.

The processing comprises of 3D pose estimation of the scanning system using Kalman Filter (KF). Later, based on the generated localisation of the system, the registration of horizontal and front vertical scan points has been carried out to develop the 3D point cloud map of the surveyed vicinity. The developed map is further used to assess environmental information such as dimensions of open spaces, locations of street furniture such as an electric pole, and the layouts of the slum region. In this work, the Revit software-based map uploading and its assessment have been performed and multiple options have been pointed to do further analysis by the end users.

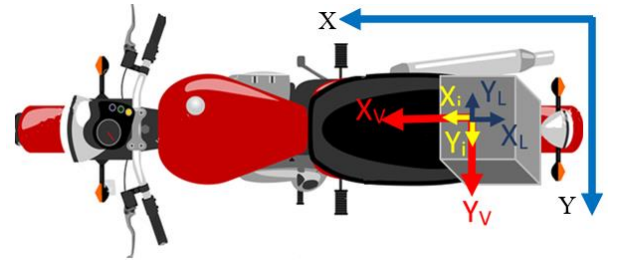


Fig. 4. Assignment of reference frames to connected sensors.

III. 3D LOCALISATION AND MAPPING USING THE MOBILE SYSTEM

In this section, we present the methodology for 3D localisation of the scanning system and the development of the 3D point cloud map of the surveyed vicinity.

A. 3D Localisation Using Kalman Filter

The performance of the mobile scanning and mapping system is mainly based on the accuracy of its localisation. The wheel encoder has been used to record the rotations of the wheel of the bike as the first source of knowledge of the motion profile. The periodically recorded encoder counts have been converted into linear displacement d_c using the known geometrical parameters of the bike wheel. This indicates the displacement that has been covered by the bike during this time stamp, as shown in Fig. 6(a). As the encoder only informs about the magnitude of the displacement vector d_c , the IMU has been utilised to perceive the angular displacements of this vector in the 3D axis. The angular displacement $\Delta\theta_{iz}$ about Z-axis is shown in Fig. 6(a). If the motion direction is in the XY plane, then the XY components of vector d_c can be obtained, as shown in brown colour in Fig. 6(a) using the IMU angular displacement for this time period. If the motion direction is in the XYZ axis, then the XYZ components of the vector d_c can be obtained using both possible angular displacements $\Delta\theta_{iy}$ and $\Delta\theta_{iz}$, as shown in brown colour in Fig. 6(b). There is no significant angular displacement observed about X axis during the normal motion of the bike; therefore, it is neglected in this work.

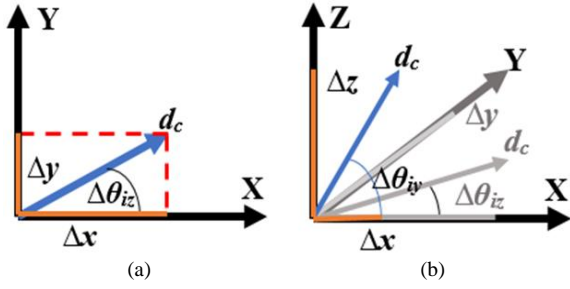


Fig. 6. Displacement vector of the motorbike: (a) Vector decomposition in 2D plane; (b) Vector decomposition in 3D plane.

Standard transformations have been applied to convert the d_c and IMU orientation data into relative 3D Cartesian coordinates for this time instant, as shown in (1)

$$\Delta \mathbf{T}_v = \mathbf{Rot}(Y, \Delta \theta_{iy}) \times \mathbf{Rot}(Z, \Delta \theta_{iz}) \times d_c. \quad (1)$$

Here the relative translational update of the bike has been represented by the vector $\Delta \mathbf{T}_v = [\Delta x \ \Delta y \ \Delta z]^T$ for any time instant. By concatenating the IMU orientation data into $\Delta \mathbf{T}_v$, the periodic odometric update $\Delta \mathbf{O}_v = [\Delta x \ \Delta y \ \Delta z \ \Delta \theta_{ix} \ \Delta \theta_{iy} \ \Delta \theta_{iz}]^T$ of the bike has been achieved. As the only odometric update cannot provide the pose information of the bike for the complete journey accurately, therefore a Kalman Filter (KF)-based localisation scheme has been applied to the recorded sensorial data [21]. The encoder and IMU data have been utilised for the prediction step of KF. The GPS, horizontal 2D laser scanner, and stereo vision data have been used in the correction step of KF. The standard KF prediction equations are shown in (2) and (3) to estimate the bike pose $X = [x \ y \ z \ \theta_x \ \theta_y \ \theta_z]^T$ and its covariance P at a given time stamp:

$$\mathbf{X}_p = \mathbf{A}\mathbf{X}_{n-1} + \Delta \mathbf{O}_v, \quad (2)$$

$$\mathbf{P}_p = \mathbf{A}\mathbf{P}_{n-1}\mathbf{A}^T + \mathbf{Q}. \quad (3)$$

Here, system Jacobean matrix A holds unity at diagonal while system noise matrix Q holds the variances of all state variables in diagonal which are provided in the datasheet of the odometric sensors. On reception of any exteroceptive sensorial information, such as GPS updates, the KF correction phase is invoked, as shown in (4) to (6):

$$\mathbf{Y}_n = \mathbf{Z}_n - \mathbf{H}\mathbf{X}_p, \quad (4)$$

$$\mathbf{S}_n = \mathbf{H}\mathbf{P}_p\mathbf{H}^T + \mathbf{R}, \quad (5)$$

$$\mathbf{K}_n = \mathbf{P}_p\mathbf{H}^T\mathbf{S}_n^{-1}. \quad (6)$$

The GPS values provide latitude and longitude coordinates of the bike, where it is moving, however, the KF implementation has been carried out solely in SI units so the GPS georeferenced coordinates received for any time stamp have been converted into metre using standard relation of one degree equals to 111 km. Therefore, the measurement vector Z_n maintains the relative coordinates of the XY plane as presented by $Z_n = [\Delta x \ \Delta y \ 0 \ 0 \ 0 \ 0]^T$. If due to obstacles, GPS data are detected as unreliable, then it has not served to correct the KF estimate. Like the A matrix, the Jacobean measurement matrix H holds unity on the diagonal because of the direct relationship among Z_n and X_p . The

variance provided in the GPS receiver datasheet has been placed in R to compute the above equations to determine the Kalman gain K_n . Later, the estimation of the state vector X_n and covariance matrix P_n for current-time samples has been carried out using (7) and (8):

$$\mathbf{X}_n = \mathbf{X}_p + \mathbf{K}_n\mathbf{Y}_n, \quad (7)$$

$$\mathbf{P}_n = (\mathbf{I} - \mathbf{K}_n\mathbf{H})\mathbf{P}_p. \quad (8)$$

In case of no further exteroceptive information, the prediction step of KF initiates again for a new time stamp to run the filter as explained. However, there are always multiple exteroceptive sensorial data streams present that appear asynchronously one after another. The most repeatable stream is the Simultaneous Localisation and Mapping (SLAM)-based environmental perception estimation using 2D laser scans. The horizontal scanner has been used to scan the XY plane of the vicinity and its live data have been utilized to run the open source Hector SLAM ROS package to produce 2D pose and the map [22]. The actual idea of the SLAM is to estimate the most probable map m and pose x by factorizing complete SLAM posterior $p(x_{1:t}, m | z_{1:t}, u_{0:t-1})$ into factored form, as shown in (9) [23]

$$p(x_{1:t}, m_{1:q} | z_{1:t}, u_{0:t-1}) = p(x_{1:t} | z_{1:t}, u_{0:t-1}) \cdot \prod_{j=1}^q p(m_j | x_{1:t}, z_{1:t}). \quad (9)$$

The estimated SLAM pose has been used to generate the measurement vector $Z_n = [\Delta x \ \Delta y \ 0 \ 0 \ 0 \ \Delta \theta_z]$ to re-initiate the KF correction phase, as shown earlier by (4) to (8). The final exteroceptive data stream has been received through a stereo camera. The camera has been used to view the region and its vision data have been utilized to run the open source Stereolab ROS package to produce 3D pose and the orientation data [24]. Figure 7(a) shows an example image of an outdoor region from where the stereo camera pose estimation has begun. Figure 7(b) shows the continuity of vision perception of the region on a slope, and the overall translational changes are shown in Fig. 8. However, it is necessary to have distinct vision features available in the explored environment in order to get satisfactory poses generated through stereo images.

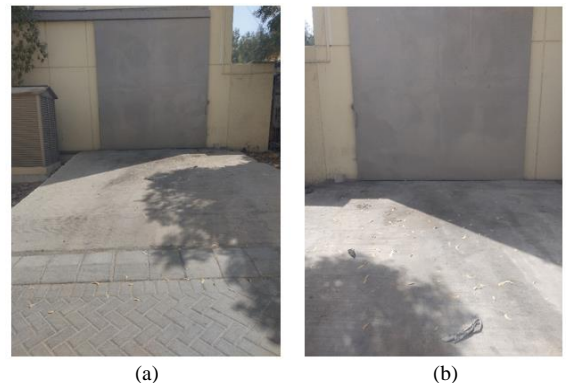


Fig. 7. Stereo vision perception in outdoor region: (a) An example image of an outdoor region from where the stereo camera pose estimation has been initiated; (b) The continuity of vision perception of the region on a slope.

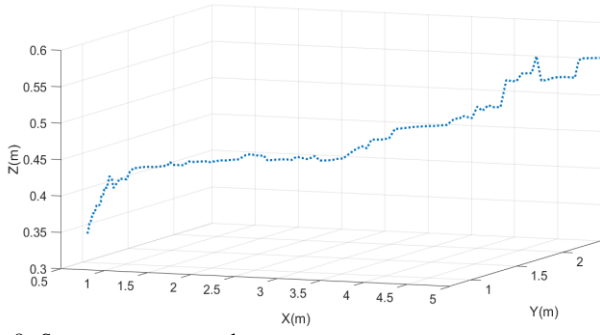


Fig. 8. Stereo camera pose values.

The estimated stereo pose has been used to generate the measurement vector $Z_n = [\Delta x \ \Delta y \ \Delta z \ 0 \ 0 \ 0]$ to re-initiate the KF correction phase. After ending the correction phase due to any of the exteroceptive sensors, the KF prediction phase will initiate again using the odometric update and continue to run again the KF correction phase.

The scanning system has been tested first on an academic block street, as shown in Fig. 9. The bike has moved in a straight path with possibly minimal speed to perceive the environmental knowledge at maximum. Using ROS packages, the online data of the horizontal scanner and stereo camera have been utilised to compute poses of the system, and all the online sensorial data have been recorded in the ROS bag file.



Fig. 9. Views of the academic block environment.

In offline processing using MATLAB scripts, the recorded data have been utilised to compute the estimated pose of the bike using KF, as shown in Fig. 10.

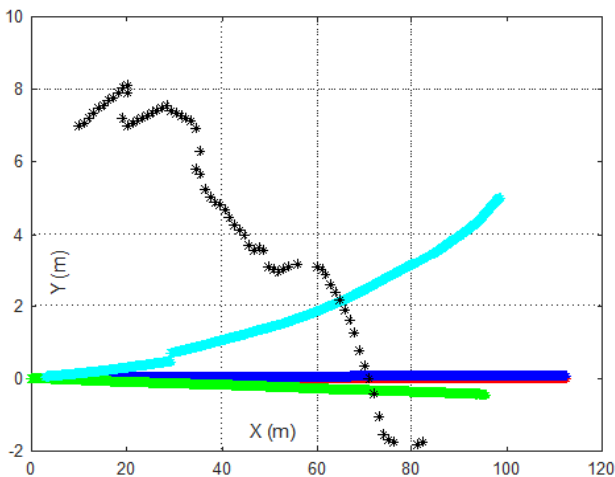


Fig. 10. Pose of the system inside the academic block environment.

The green line shows the odometric pose of the bike that has been used in the prediction step of KF. The blue line shows the SLAM pose of the bike that has been utilised in the KF correction step. Due to availability of distinct structural shapes, the SLAM pose has been found to be quite satisfactory. The estimated KF pose is shown in red line, which is almost overlapped with the SLAM pose. On the other hand, the GPS data were not as reliable in this test due to the presence of trees and obstacles, as shown by black marks. In each iteration of KF, the sensorial data have been closely checked through some thresholds before passing them to prediction or correction steps. Therefore, GPS data have not been thoroughly utilized in this test. Similarly, the stereo poses have also started to deviate after certain surveying operation, as shown by the cyan line, and therefore they have not been fully utilised throughout the test. The KF estimated pose has been utilised for the development of the 3D point cloud map of the environment.

B. 3D Point Cloud Map Development

The azimuth XY plane environmental perception has been achieved through horizontal 2D laser scanner and using the estimated poses in red colour, as shown in Fig. 11, the 2D map has been developed of the surveyed vicinity.

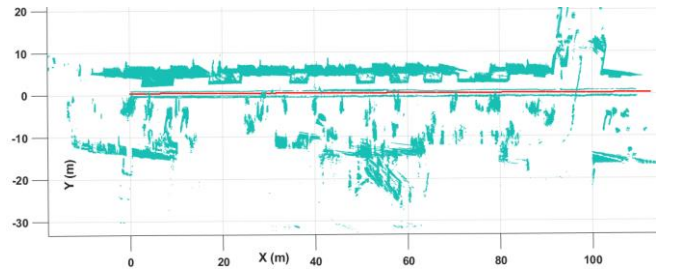


Fig. 11. 2D map of the academic block environment.

The 3D environment perception has been achieved using a vertical 2D laser scanner. The scanner has been utilised to scan the XZ plane of the surveyed vicinity. Therefore, the gathered scan is required to be transformed into the 3D reference axis of the moving system. So, each scan point P_{S2} of the vertical scanner has been transformed using a standard transformation procedure, as shown by (10)

$$\mathbf{P}_{sv} = \text{Trans}(\Delta x_v, \Delta y_v, \Delta z_v) \times \text{Rot}(\mathbf{Z}, \Delta \theta_{vz}) \times \text{Rot}(\mathbf{Y}, \Delta \theta_{vy}) \times \mathbf{P}_{S2}. \quad (10)$$

Here, P_{sv} is the transformed 3D scan point in the bike reference frame, the Δx_v , Δy_v , Δz_v are the translational values where the origin of the vertical scanner has been placed with respect to the reference frame, and $\Delta \theta_{vy}$ and $\Delta \theta_{vz}$ are the angular displacements of the vertical scanner mounting with respect to the reference frame of the bike. Each transformed scan point P_{sv} has been concatenated to make the complete scan S_{TV} . Now, using the estimated poses at respective time, the complete scan S_{TV} can be registered into the world coordinated system to incrementally generate a consistent 3D point cloud map. The final transformation of the complete scan into these coordinates is shown in (11)

$$\mathbf{S}_{TW} = \text{Trans}(\mathbf{x}, \mathbf{y}, \mathbf{z}) \times \text{Rot}(\mathbf{Z}, \theta_z) \times \mathbf{S}_{TV}. \quad (11)$$

Here S_{TW} is the transformed scan w.r.t. the world coordinate system. Respective time stamped translational (x, y, z) and rotational (θ_z) pose values related to movement of the bike have been used for the transformation. The process of transformation of each scan has been repeated for all vertical scans. By accumulating all these scans recorded at different time stamps with their respective pose information, the final 3D point cloud map has been generated in offline mode, as shown in Fig. 12.

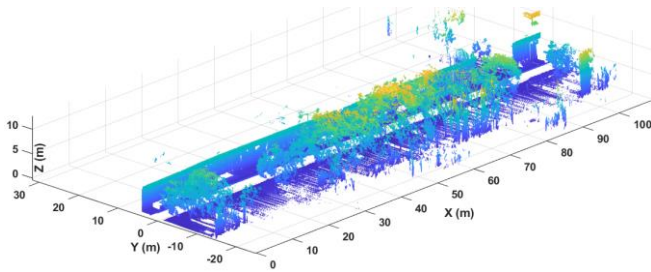


Fig. 12. 3D point cloud of the academic block environment.

The generated point cloud represents the scanned vicinity of $120 \times 50 \times 12 \text{ m}^3$ dimension and shows detailed information about structure, vegetation, and open spaces. The time taken for scanning the environment was approximately two minutes and time consumed for developing the point cloud was roughly fifty minutes, which reflects the benefits of scanning and mapping technology that a comprehensive information of surveyed vicinity can be gathered quickly. Further, the developed map can be used for assessment of unique objects and open spaces. The Autodesk ReCap software has been used to explore the map of the surveyed region, as shown in Fig. 13 [25].

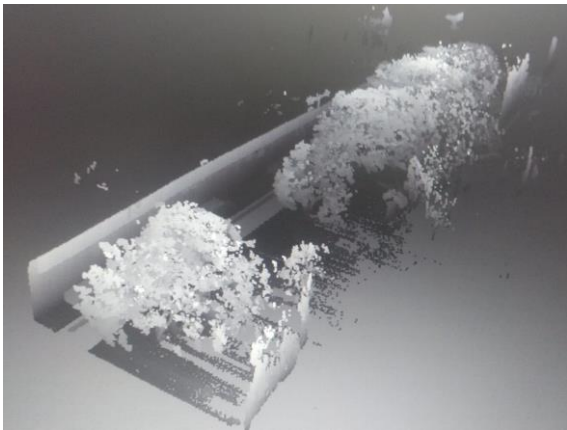


Fig. 13. 3D point cloud map view inside the Recap.

Multiple dimensions of the region can be determined using simple tools provided in the software. The length and width of selected path are shown in the top view of the region in Fig. 14.



Fig. 14. Dimensions of open spaces determined inside Recap.

The dimensions of a tree and an electric pole have been

determined with the usage of tools and are shown in Fig. 15.

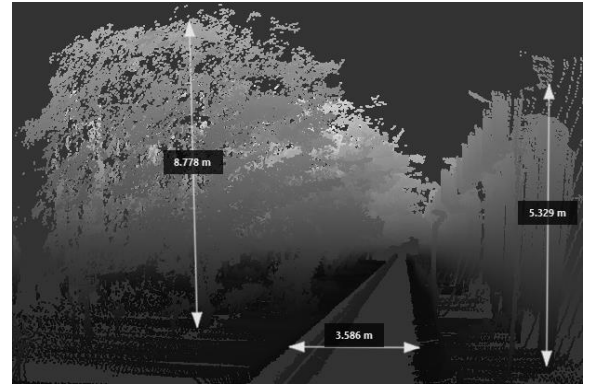


Fig. 15. Dimensions of street objects determined inside Recap.

The dimensions of the developed point cloud have been found accurate as compared to ground truth as presented in Table I.

TABLE I. COMPARISON OF MEASURED RESULTS.

Object	Open Space		Electric Pole	
	Actual	Measured	Actual	Measured
Length (m)	115	114	-	-
Width (m)	3.7	3.58	0.4	0.25
Height (m)	-	-	5.5	5.32

Therefore, the efficacy of the developed mapping system and ease of assessment using dedicated software have been found remarkable. The overall mechanism is quite helpful for aiding the relevant industries and agencies.

IV. RESULTS

The motorbike-based scanning system has been further tested in various real environments. The second real test has been carried out inside a long slum vicinity, as shown in Fig. 16.



Fig. 16. Views of the slum region.

The vicinity has many tent units with no standard structures and constructed in disorder. Most tents have very small dimensions, and only some structures have proper elevation. The movement of the bike was quite challenging and slow; at least twice, the surveyor did the trip due to a failure of not properly running the bike on uneven terrain in the presence of random crossing of inhabitants. However, in the second attempt, the survey was performed successfully, indicating the achievement of the slim scanning prototype over larger car-based scanning systems [14]. Even the presented scanning prototype has shown no issues with

random hanging of electric or cable wires passing at low heights, which is a greater challenge for some state-of-the-art motorbike-based scanning systems [26].

All sensorial data have been recorded during the bike movement and it is observed that both SLAM and GPS measurements have been correctly recorded, however, the stereo vision was not completely successful until the end of surveying. Therefore, pose estimation has been done using odometric updates and by SLAM and GPS corrective measurements. Using the estimated localisation, the 3D point cloud of the region has been developed, as shown in Fig. 17.

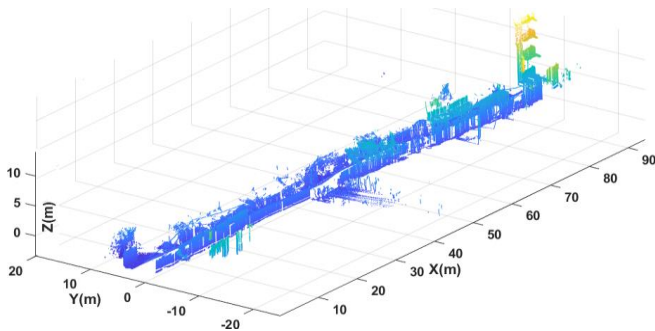


Fig. 17. 3D point cloud map of the vicinity of the slum.

The developed point cloud is utilised in the Recap software, as shown in Fig. 18 to identify its dimensions.

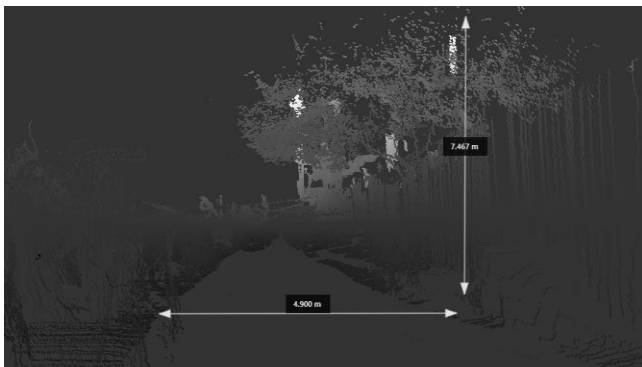


Fig. 18. Dimensions of open spaces determined using Recap.

The developed point cloud represents small tent houses, few cemented structures with improper construction present in the slum, a rare plantation, and even shows hanging cables if observed minutely. Disordered streets and ultra small open spaces have been observed and measured in the Recap software. The width of the selected open space and the height of the tallest tree have been identified, as shown in Fig. 18. The total length of the surveyed region has been determined and shown in Fig. 19. The dimensions of the developed point cloud have been compared with the ground truth, as shown in Table II, and found to be nearly accurate. Keeping in view the performance of the state-of-the-art motorbike scanning system [26], the results developed of the slim prototype scan system presented are quite satisfactory and acceptable to the surveyors.

TABLE II. COMPARISON OF MEASURED RESULTS.

Region	Slum tent area		Small street area	
	Actual	Measured	Actual	Measured
Length (m)	69	66	40	35.8
Width (m)	5.2	4.9	6	5.8

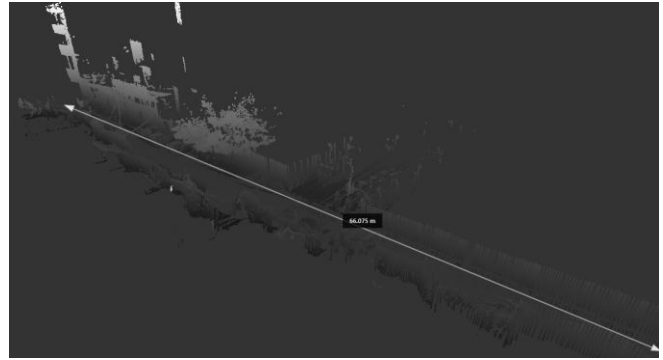


Fig. 19. Determination of length of the slum territory surveyed.

The scanning system has been finally tested in a highly populated low-income urban dense region, as shown in Fig. 20. The vicinity has many small housing units with multiple floors developed in small streets. The movement of the bike was again difficult due to continuous movements of the residents in the streets; however, the surveyor did his best to capture the environmental knowledge.

All the sensorial data have been recorded during the bike movement and it is observed that only SLAM measurements have been correctly generated. Other GPS positioning data were not received accurately due to a very limited view of the open sky. Similarly, the stereo vision-based positioning data were quite inaccurate due to unavailability of the dominant vision features inside the captured images. Therefore, the pose estimation has been done using odometric updates and by SLAM corrective measurements. Using the estimated localisation, the 3D point cloud of the region has been developed, as shown in Fig. 21.



Fig. 20. Views of the densely populated region.

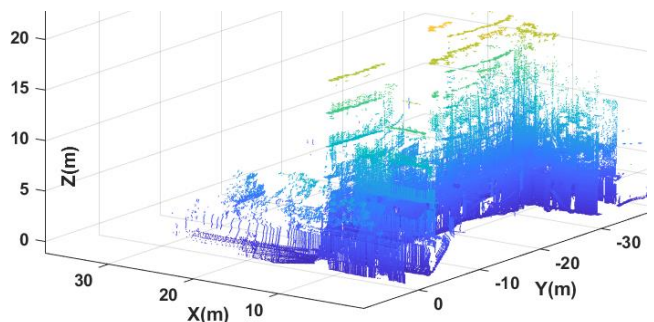


Fig. 21. 3D point cloud map of the surveyed vicinity.

The point cloud represents small streets and compact

multi-floor housing units. Cabling and wiring are randomly observed above open spaces. The width and length of the open space have been determined using the Recap tools, as shown in Fig. 22.

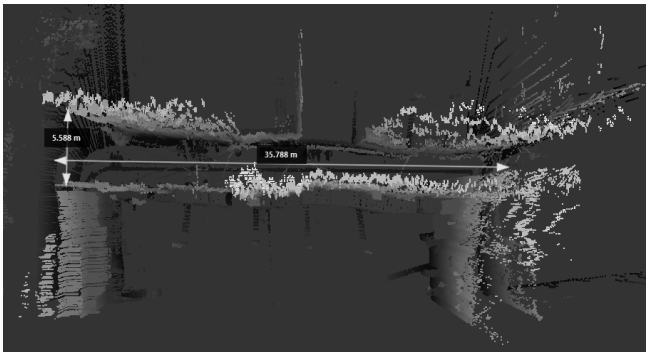


Fig. 22. Dimensions of open spaces determined using Recap.

A sample of the street and the connecting cables are shown in Fig. 23. The height of a pair of cables is determined and pointed in the mentioned figure. A portion of the floor along the stairs elevation has also been examined in the software and is shown in Fig. 23.

The developed point cloud has been compared with the ground truth, as shown in Table II, and found to be nearly accurate.

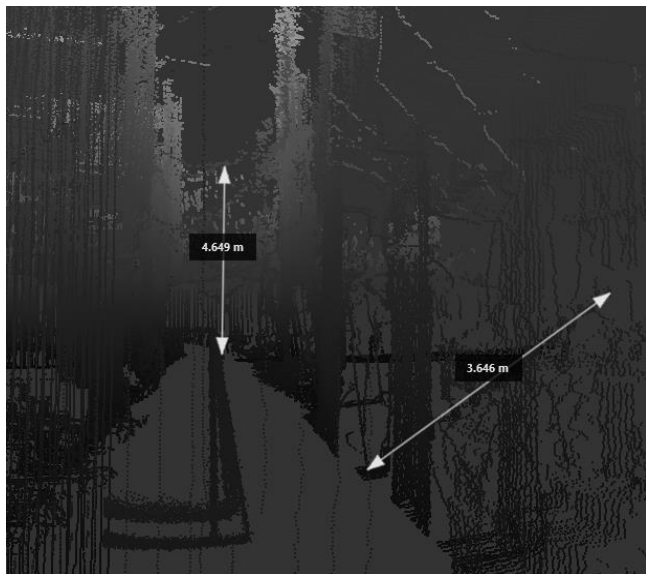


Fig. 23. Determination of dimensions of the selected territory.

The test results have been presented for multiple slums and densely populated regions. There were some certain regions where the scan had not been performed properly, mainly due to crowd movement and narrow streets. Therefore, this is still a quite interesting work under progress to facilitate the related governmental or semi-governmental agencies to provide useful survey results.

V. CONCLUSIONS

This research work presented the working of an efficient orthogonally configured motorbike-based scanning system. The developed mapping results of the system have been found to be 94 % accurate if compared with the actual dimensions of surveyed vicinities. The time taken to generate survey results has been minimised to 90 % or more

with ease of operation at affordable rates compared with the available survey techniques in the regional market. In addition, the mapping results have been further analysed with relevant software to assess the map and the targeted objects, present within the map. To improve the localisation and visualisation of the surveyed regions, the use of recorded monocular vision information has been planned in future work with the latest classification and segmentation techniques.

ACKNOWLEDGMENT

The authors thank staff of the Department of Electronic Engineering, NEDUET, for their continuous help and support.

CONFLICTS OF INTEREST

The authors declare that they have no conflicts of interest.

REFERENCES

- [1] Y. Shi, M. Bilal, H. C. Ho, and A. Omar, "Urbanization and regional air pollution across South Asian developing countries – A nationwide land use regression for ambient PM_{2.5} assessment in Pakistan", *Environmental Pollution*, vol. 266, part 2, art. 115145, 2020. DOI: 10.1016/j.envpol.2020.115145.
- [2] G. Lenda, A. Uznanski, M. Strach, and P. Lewinska, "Laser scanning in engineering surveying: Methods of measurement and modeling of structures", *Reports on Geodesy and Geoinformatics*, vol. 100, no. 1, 2016. DOI: 10.1515/rgg-2016-0010.
- [3] A. P. Spring, "A history of laser scanning, Part 1: Space and defense applications", *Photogrammetric Engineering and Remote Sensing*, vol. 86, no. 7, pp. 419–429, 2020. DOI: 10.14358/PERS.86.7.419.
- [4] A. P. Spring, "A history of laser scanning, Part 2: The later phase of industrial and heritage applications", *Photogrammetric Engineering and Remote Sensing*, vol. 86, no. 8, pp. 479–501, 2020. DOI: 10.14358/PERS.86.8.479.
- [5] L. Klingbeil, C. Eling, E. Heinz, and M. Wieland, "Direct georeferencing for portable mapping systems: In the air and on the ground", *Journal of Surveying Engineering*, vol. 143, no. 4, 2017. DOI: 10.1061/(ASCE)SU.1943-5428.0000229.
- [6] S. Chakravarty, "Here are top mobile mapping systems that would interest you", *Geospatial World*, 2018. [Online]. Available: <https://www.geospatialworld.net/blogs/here-are-five-mobile-mapping-systems-that-would-interest-you/>
- [7] S. R. un N. Jafri *et al.*, "Campus terrain surveying and mapping using low range 2D laser scanners", in *Proc. of 2021 Seventh International Conference on Aerospace Science and Engineering (ICASE)*, 2021, pp. 1–6. DOI: 10.1109/ICASE54940.2021.9904233.
- [8] Velodyne 3D Laser Scanners. [Online]. Available: <https://velodynelidar.com/products/puck/>
- [9] Sick 2D Laser Scanners. [Online]. Available: <https://www.sick.com/us/en/lidar-sensors/2d-lidar-sensors/tim/c/g570093>
- [10] Hokuyo 2D Laser Scanners. [Online]. Available: www.robotshop.com/en/hokuyo-utm-03lx-laser-scanning-range-finder.html
- [11] K. Xing, X. Zhang, Y. Lin, W. Ci, and W. Dong, "Simultaneous localization and mapping algorithm based on the asynchronous fusion of laser and vision sensors", *Frontiers in Neurorobotics*, vol. 16, 2022. DOI: 10.3389/fnbot.2022.866294.
- [12] T. Lovas, K. Hadzijanisz, V. Papp, and A. J. Somogyi, "Indoor building survey assessment", *International Archives of the Photogrammetry, Remote Sensing and Spatial Information Sciences*, vol. XLIII-B1-2020, 2020. DOI: 10.5194/isprs-archives-XLIII-B1-2020-251-2020.
- [13] S. R. un N. Jafri, Y. Rehman, S. M. Faraz, H. Amjad, M. Sultan, and S. J. Rashid, "Development of georeferenced 3D point cloud in GPS denied environments using backpack laser scanning system", *Elektronika ir Elektrotechnika*, vol. 27, no. 6, pp. 25–34, 2021. DOI: 10.5755/j02.eie.29063.
- [14] A. Escola *et al.*, "Mobile terrestrial laser scanner applications in precision friculture/horticulture and tools to extract information from canopy point clouds", *Precision Agriculture*, vol. 18, pp. 111–132, 2017. DOI: 10.1007/s11119-016-9474-5.

- [15] L. Garberoglio, P. Moreno, I. Mas, and J. I. Giribet, "Autonomous vehicles for outdoor multidomain mapping", in *Proc. of IEEE Biennial Congress of Argentina (ARGENCON)*, 2018, pp. 1–8. DOI: 10.1109/ARGENCON.2018.8646054.
- [16] K. Sidharth, N. Menon, A. Sadique, and P. Lalu, "Sensor fusion, mapping, localization and calibration of a converted autonomous quad bike", in *Proc. of SAE International Conference on Advances in Design, Materials, Manufacturing and Surface Engineering for Mobility*, 2022. DOI: 10.4271/2022-28-0561.
- [17] O. Elkady, "SLAM for smart bikes", B.A. thesis, University of Twente, Netherlands, 2022. [Online]. Available: <https://essay.utwente.nl/91987/>
- [18] M. Renee, "Design and application of lidar systems and electric bicycle modeling for transportation safety", Ph.D. dissertation, University of Kansas, 2021.
- [19] K. Tokorodani, M. Hashimoto, Y. Aihara, and K. Takahashi, "Point-cloud mapping using lidar mounted on two-wheeled vehicle based on NDT scan matching", in *Proc. of International Conference on Informatics in Control, Automation and Robotics*, 2019. DOI: 10.5220/0007946204460452.
- [20] S. Stasinopoulos, M. Zhao, and Y. Zhong, "Simultaneous localization and mapping for autonomous bicycles", *International Journal of Advanced Robotic Systems*, vol. 14, no. 3, pp. 1–16, 2017. DOI: 10.1177/1729881417707170.
- [21] I. Ullah, X. Su, X. Zhang, and D. Choi, "Simultaneous localization and mapping based on Kalman Filter and Extended Kalman filter", *Wireless communications and Mobile computing*, vol. 2020, art. ID 2138643, 2020. DOI: 10.1155/2020/2138643.
- [22] S. Kohlbrecher, O. von Stryk, J. Meyer, and U. Klingauf, "A flexible and scalable SLAM system with full 3D motion estimation", in *Proc. of 2011 IEEE International Symposium on Safety, Security, and Rescue Robotics*, 2011, pp. 155–160. DOI: 10.1109/SSRR.2011.6106777.
- [23] S. Thrun, W. Burgard, and D. Fox, *Probabilistic Robotics*. MIT Press, 2005.
- [24] Stereolabs. [Online]. Available: <https://www.stereolabs.com/docs/ros/>
- [25] Autodesk Recap. [Online]. Available: <https://www.autodesk.com/products/recap/features>
- [26] Z. Yan, R. Liu, L. Cheng, X. Zhou, X. Ruan, and Y. Xiao, "A concave hull methodology for calculating the crown volume of individual trees based on vehicle-borne LiDAR data", *Remote Sensing*, vol. 11, no. 6, p. 623, 2019. DOI: 10.3390/rs11060623.



This article is an open access article distributed under the terms and conditions of the Creative Commons Attribution 4.0 (CC BY 4.0) license (<http://creativecommons.org/licenses/by/4.0/>).